Journal of Hazardous Materials 162 (2009) 530–535

Contents lists available at ScienceDirect

Journal of Hazardous Materials

journal homepage: www.elsevier.com/locate/jhazmat

Experimental and numerical investigations of effect of column length on retardation factor determination: A case study of cesium transport in crushed granite

Ming-Hsu Li[a,*], Tsing-Hai Wang[b], Shi-Ping Teng[b]

[a] Institute of Hydrological and Oceanic Sciences, National Central University, #300 Jhongda Road, Jhongli City, 320, Taiwan
[b] Department of Engineering and System Science, National Tsing Hua University, Taiwan

ARTICLE INFO

Article history:
Received 31 January 2008
Received in revised form 25 April 2008
Accepted 16 May 2008
Available online 21 May 2008

Keywords:
Cesium
Crushed granite
Retardation
Column experiment

ABSTRACT

This study investigated breakthrough curves (BTCs) from a series of column experiments, including different column lengths and flow rates, of a conservative tracer, tritium oxide (HTO), and a radionuclide, cesium, in crushed granite using a reactive transport model. Results of the short column, with length of 2 cm, showed an underestimation of the retardation factor and the corresponding HTO BTCs cannot be successfully modeled even with overestimated fluid dispersivity. Column supporting elements, including filters and rings, on both ends of packed granite were shown to be able to induce additional dispersive mixing, thus significantly affecting BTCs of short columns while those of the long column, with length of 8 cm, were less affected. By increasing flow rates from 1 mL/min to 5 mL/min, the contribution of structural dispersive mixing to the false tilting of short column BTCs still cannot be detached. To reduce the influence of structural dispersivity on BTCs, the equivalent pore volume of column supporting materials should be much smaller than that of packed porous medium. The total length of column supporting structures should be greatly shorter than that of porous medium column.

1. Introduction

The fate and transport of radionuclides in geological substances have been widely studied because radionuclide residues in aquatic and geological environments may accumulate in microorganisms and enter into human food chain [1–5]. The key to accurately estimating radionuclide transport for safety assessment programs relies on the validity of physical and chemical parameters used for performance evaluations. Among numerous techniques applied in the field and laboratory, the advection–dispersion column experiments are frequently utilized to evaluate the migration of concerned contaminants transporting through porous media [6,7]. For example, the retardation factor can be estimated by comparing the arrival time of breakthrough curves (BTCs) between a radionuclide and a conservative tracer. The conservative tracer is an inert analog of species having no chemical interactions with the filled porous medium, whereas the radionuclide will undertake chemical reactions affecting the transport of radionuclides in geological environments. The BTCs are concentration time series observed from effluent solutions of column experiments. Owing to the inert nature of conservative tracers, only physical transport will affect the BTCs tilting of conservative tracers. On the contrary, the radionuclides BTCs represent a mixture of physical transport and chemical reactions. The main advantage of column experiments is simply that in situ hydrogeological conditions can be approximately reconstructed in laboratories [8]. Meanwhile, the main disadvantage is that they are frequently time consuming and involve mixing of chemical and physical transport processes on the measured BTCs. Without correctly identifying the contribution of physical transport on the BTCs of reactive species in advance, chemical parameters determined herein will be seriously contaminated by inheriting over/under estimations of physical transport processes.

Regarding the need of rapidly achieving experimental results, short columns are generally the preferred choices simply because the speed of obtaining BTCs increases with reducing column length, especially time consuming through-diffusion experiments. For example, the diffusion coefficient of most cations or anions lies in the magnitude of 10^{-9}–10^{-12} m/s, showing an intensive experimental time of nearly one year is required to obtain a complete breakthrough of a 2 cm column. The lengths of the packed substance columns ranged from 2 cm to 200 cm and the column diameters varied from 2.5 cm to 7.5 cm [6,9–15]. In spite of differences in column lengths, few works are aimed to examine the validity of parameters determined with different column lengths

* Corresponding author. Tel.: +886 3 4222964; fax: +886 3 4222964.
E-mail address: mli@cc.ncu.edu.tw (M.-H. Li).

0304-3894/$ – see front matter © 2008 Elsevier B.V. All rights reserved.
doi:10.1016/j.jhazmat.2008.05.076

or flow rates in one study. The question is whether parameters determined from a single column experiment can be validated for future in situ applications if parameters determined from different column lengths or flow rates were inconsistent with each other.

Both a conservative tracer, tritium oxide (HTO, half live ~12.3 years), and a radionuclide, cesium (^{137}Cs, half live ~30 years), were applied to two lengths of advection–dispersion columns at two flow rates, 1 mL/min and 5 mL/min, of synthetic groundwater and seawater. Numerical experiments were performed to explain the discrepancies in physical parameters between the short and long columns and examine the validity of the sorption parameter, the retardation factor, based on experimental BTCs.

2. Material and methods

2.1. Solid and liquid phases

Granite is a potential host rock at a future waste disposal site in Taiwan and could be ground for use as a backfill material. Fresh (unweathered) granite was sampled from an experimental borehole with a depth of 177–178 m below ground surface located on an islet in the Taiwan Strait. The sampled granite was crushed and washed with deionized water in an ultrasonic bath to remove fine particles and then dried and stored in an oven at a temperature of 60 °C. The particle size of the crushed granite selected in this study is between #60 and #80 meshes, 0.25 mm and 0.18 mm, respectively. The primary constituent minerals identified by the X-ray diffraction (Philips PW1300) are quartz, biotite, augite, muscovite, and lepidolite. Meanwhile, the predominant species were determined by inductively coupled plasma mass spectroscopy (Sciex Elan 5000, PerkinElmer) as being SiO_2 (72.6%), Al_2O_3 (12.9%), K_2O (8.8%), Na_2O (4.2%) and Fe_2O_3 (1.1%). Two synthetic liquid phases, groundwater (GW) and seawater (SW), were prepared with the compositions listed in Table 1. The concentration of ^{137}Cs was prepared at 1×10^{-4} mol/L using the radioactive tracer of ^{137}Cs ion from Amersham.

2.2. Advection–dispersion column experiment

The schematic structure of the Teflon column used in this study was depicted in Fig. 1. A total of four columns, two for each length of 2 cm and 8 cm, were fabricated with an identical diameter of 5 cm. One set of 2 cm and 8 cm columns is used for GW and the other set for SW. The crushed granite particles were evenly spread layer by layer and compressed inside the columns to ensure consistent bulk density and porosity, which were calculated as 1.45 g/cm^3 and 0.55, respectively. Filter papers (30 μm, Advantec) were added to the top and bottom sides of the packed crushed granite to prevent granite particle release. Additional Teflon filters with 36 equally spaced pin holes at a thickness of 0.8 cm associated with Teflon rings at a thickness of 0.8 cm were fabricated next to the filter paper as supporting materials. These additional Teflon components provided further support for the filter papers against the high pressure induced by fluid flows. The column was completed using Teflon lids and inlet/outlet valves on both ends.

Table 1
The composition and concentration of synthetic groundwater (GW, pH 7.12) and seawater (SW, pH 7.32)

	GW (mol/L)	SW (mol/L)
Cl^-	1.78×10^{-1}	5.50×10^{-1}
Br^-	5.01×10^{-4}	8.39×10^{-4}
F^-	8.00×10^{-5}	6.80×10^{-5}
HCO_3^-	1.64×10^{-4}	–
SO_4^{2-}	5.83×10^{-3}	2.81×10^{-2}
BO_3^{3-}	–	4.16×10^{-4}
Na^+	9.13×10^{-2}	4.70×10^{-1}
K^+	2.07×10^{-4}	1.02×10^{-2}
Li^+	1.44×10^{-4}	2.50×10^{-5}
Ca^{2+}	4.72×10^{-2}	1.03×10^{-2}
Mg^{2+}	1.73×10^{-3}	5.31×10^{-2}
Sr^{2+}	4.00×10^{-4}	8.70×10^{-5}

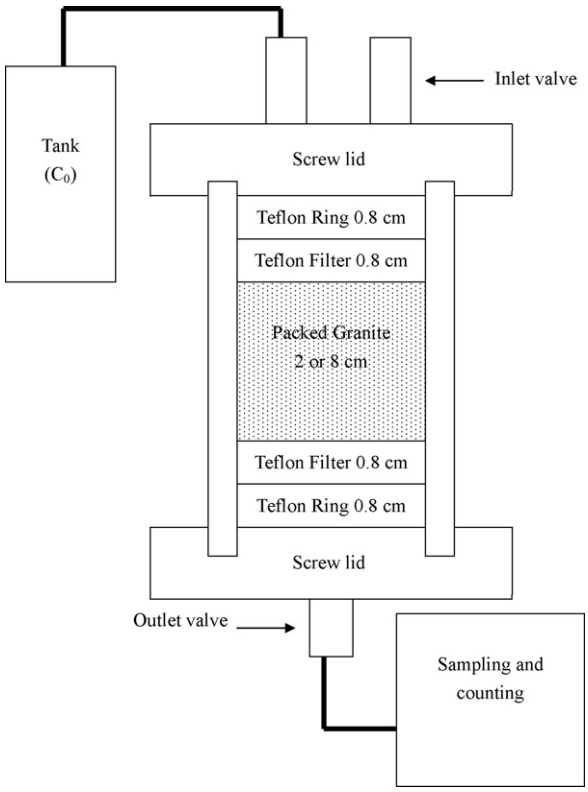

Fig. 1. The schematic structure of column setup. All parts are made up of Teflon with a column inner-diameter of 5 cm.

Prior to conducting further experiments, one set of packed granite columns (2 cm and 8 cm) was first saturated by cycling fresh GW for 7 days using a peristalsis pump, while the other set of columns was saturated with fresh SW solutions with another pump. The purpose of GW and SW saturations is to ensure the surface chemistry of packed granite particles to be equilibrated as similar to those observed in the field. More importantly, the cycling process of saturation is to stabilize fine pores of packed granite particles against possible cracking induced by fluid flows.

The advection–dispersion experiments were first performed using HTO in both GW and SW at a flow rate of 1 mL/min, and then with Cs in both solutions. After flushing fresh GW or SW solutions through these columns until no detectable radioactivity of Cs in effluents, the experiments were performed again at a flow rate of 5 mL/min. As a result, a total of 16 experimental BTCs (2 column lengths × 2 species × 2 solutions × 2 flow rates) were measured. The effluent HTO solutions were collected and mixed with cocktail (liquid scintillation solution, Amersham) and their beta-ray activities were then measured by liquid scintillation dosimeter (Liquid scintillation analyzer, 2560 TR/XL, Packard). The gamma-ray activities of Cs effluent were directly counted by an NaI(Tl) detector (Wallac 1470 Wizard). The normalized activities of HTO and Cs concentrations (i.e., the activity of effluent/the activity of stock solutions) were thus obtained.

The experimental retardation factor can be estimated by comparing the migration distances between conserved and adsorbed species after time t, at concentrations where $C/C_0 = 0.5$ [16]. The

comparison of time values reaching $C/C_0 = 0.5$ from the BTCs between conserved and adsorbed species is equivalent to the comparison of migration distances when the same flow rate is applied to both conserved and adsorbed species. Consequently, the retardation factor, R, can be estimated as the time ratio of Cs reaching the relative concentrations (C/C_0) of 0.5 to HTO reaching 0.5 relative concentration (i.e., $R = T_{Cs}/T_{HTO}$).

2.3. Reactive transport modeling

To simulate experimental BTCs of HTO and Cs, the governing equation of the advection–dispersion column experiments can be given as [17],

$$\frac{\partial C}{\partial t} + \frac{\rho_b}{\theta}\frac{\partial S}{\partial t} = -V\frac{\partial C}{\partial X} + D\frac{\partial^2 C}{\partial X^2} \quad (1)$$

where C is the concentration of contaminant in solution (mol/L) and S is the amount of adsorbed contaminant on solids (mol/kg-solid), V is the pore velocity (dm/h), D is the hydrodynamic dispersion coefficient (dm^2/h), ρ_b is the bulk density (kg/dm^3), θ is the volumetric water content (dm^3/dm^3), t is time (h), and X is the distance along the column (dm). To solve Eq. (1) in a situation involving two unknowns, C and S, the retardation factor, R, can be introduced as follows,

$$R = 1 + \frac{\rho_b}{\theta}\frac{dS}{dC} \quad (2)$$

The distribution coefficient, K_d (mL/g), is related to the R value as follows,

$$R = 1 + \frac{\rho_b}{\theta}K_d \quad (3)$$

The hydrodynamic dispersion coefficient is given as follows,

$$D = \alpha_L V + \tau D_0 \quad (4)$$

where D_0 is the molecular diffusion coefficient (dm^2/h), τ is the porous medium tortuosity (dimensionless), and α_L is the longitudinal dispersivity (dm). Incorporating Eqs. (2) and (3) into Eq. (1) yields the following,

$$\left(1 + \frac{\rho_b}{\theta}K_d\right)\frac{\partial C}{\partial t} + V\frac{\partial C}{\partial X} - D\frac{\partial^2 C}{\partial X^2} = 0 \quad (5)$$

A generic reactive transport model (LEHGC) [17] is applied to solve Eq. (5) using the finite element discretization in space and the fully implicit scheme in time and decouples advection and dispersion terms with the Lagrangian–Eulerian algorithm. The BTCs of nonreactive HTO were fitted with a K_d value of zero to determine the dispersivity before determining the distribution coefficients of radioactive Cs transport [12,15]. The numerical K_d values of Cs were determined in a trial-and-error process by fitting the experimental BTCs of Cs with modeling practices. The process is end when no further significant improvement can be made. The numerical R values of C_S were then estimated using Eq. (3). To minimize discrepancies resulting from numerical errors owing to discretizations, a fixed grid size of 0.002 dm and a consistent time step size of 0.002 h were applied for all column simulations.

3. Results and discussions

3.1. Comparison of the BTCs between 2 cm and 8 cm columns

The measured BTCs for GW and SW solutions are plotted in Figs. 2 and 3, respectively. These figures present three general features. First, the breakthroughs of HTO occur faster than those of Cs in GW solution owing to the nonreactive nature of HTO. Second, the longer the packed crushed granite is, the more time the Cs requires

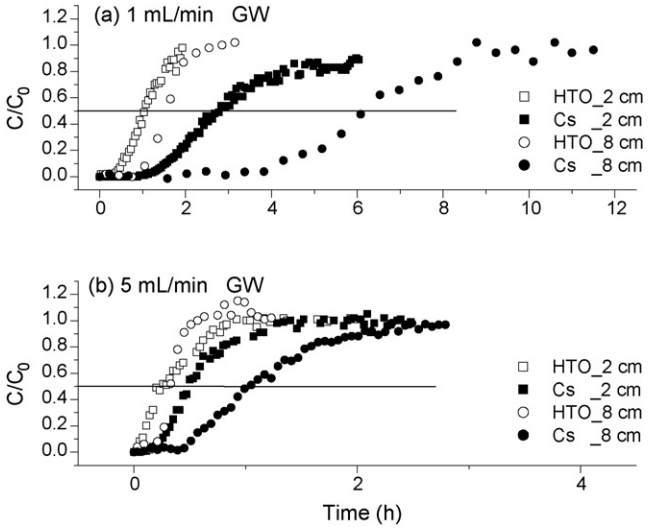

Fig. 2. The experimental BTCs of HTO and Cs with GW solutions from 2 cm and 8 cm columns. The horizontal line indicates the relative concentration of 0.5.

to achieve a breakthrough. Finally, the observed breakthroughs of Cs in the SW solution are considerably faster than those in the GW solution owing to the impeded sorption resulting from the high potassium concentration in SW (Table 1). Consequently, the BTCs of HTO and Cs in SW are similar to each other at both flow rates, as shown in Fig. 3. It is noted that the times required for HTO and Cs in GW to reach breakthrough with long and short columns are not compatible to the column lengths (Fig. 2). The results of the GW cases deserve further analyses.

The horizontal lines drawn in Figs. 2 and 3 indicate the relative concentration $C/C_0 = 0.5$. The time values of T_{Cs} and T_{HTO} were interpolated from experimental data and applied to compute the R values, as listed in Table 2. For example, the time required for HTO BTC to reach 0.5 relative concentration in 2 cm column at 1 mL/min flow rate is 1.03 h (=T_{HTO}), while that of cesium is 2.78 h (=T_{Cs}). The experimental R value is calculated as 2.78 h/1.03 h = 2.70. As listed in Table 2, the R values of Cs in GW are 2.70 and 1.96 with the 2 cm column for slow and fast flow rates, respectively, and are 3.80 and 3.18 with the 8 cm column for slow and fast flow rates, respectively. For

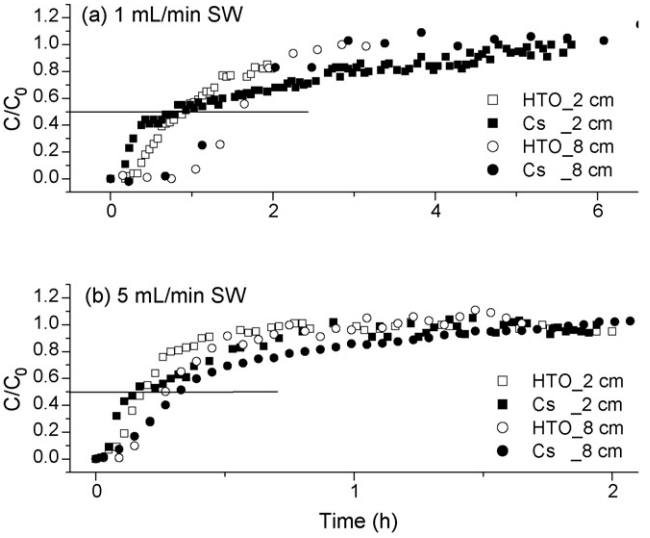

Fig. 3. The experimental BTCs of HTO and Cs with SW solutions from 2 cm and 8 cm columns. The horizontal line indicates the relative concentration of 0.5.

Table 2
The experimental results of 2 cm and 8 cm columns with fast and slow flow rates in GW and SW solutions

Solution	Flow rate (mL/min)	2 cm			8 cm		
		T_{HTO}[a] (h)	T_{Cs}[a] (h)	R	T_{HTO}[a] (h)	T_{Cs}[a] (h)	R
GW	1	1.03	2.78	2.70	1.58	6.01	3.80
	5	0.24	0.47	1.96	0.33	1.05	3.18
SW	1	0.86	0.80	0.93	1.60	1.51	0.94
	5	0.15	0.18	1.20	0.27	0.33	1.22

[a] T_{HTO} and T_{Cs} are the time values of HTO and Cs, respectively, reaching the relative concentration of 0.5 from experimental BTCs.

cases involving SW solution, the experimental R values are determined to be around 1.0 because of impeded Cs sorption from high potassium concentration. Although R values should be independent of flow rate, the experimental R values are slightly affected by changing flow rate, yet such variations are acceptable. Notably, in GW cases the R values of long columns consistently exceed those of short columns, implying inconsistent distribution coefficients (K_d) as affected by the column lengths. This phenomenon contradicts the fundamental assumption that the distribution coefficient should be independent of column length scale. Numerical experiments were performed to investigate the causes of inconsistent K_d values.

3.2. Modeling BTCs of HTO

The molecular diffusion coefficient, D_0, of HTO was selected as 10^{-4} dm^2/h [18,11,19]. Owing to the nonreactive nature of HTO, the observed tilt BTCs (Fig. 4) can be solely attributed to hydrodynamic dispersion. By adjusting the dispersivity range from 0 dm to 2 dm to numerically fit the HTO BTCs, no acceptable results can be obtained as illustrated in Fig. 4 for all 2 cm cases, including GW/SW and slow/fast flow rates. Even by setting the dispersivity as high as 2 dm, at least as one order of magnitude exceeding the level given in any of the literatures [18,20,21], results of early breakthrough were obtained with unmatched tilting patterns. As shown in Fig. 4(b) of the fast flow rate corresponding to strongly advective transport, it remains impossible to reasonably fit the HTO BTCs. Thus it is interesting to observe whether the 8 cm HTO BTCs can be reasonably simulated.

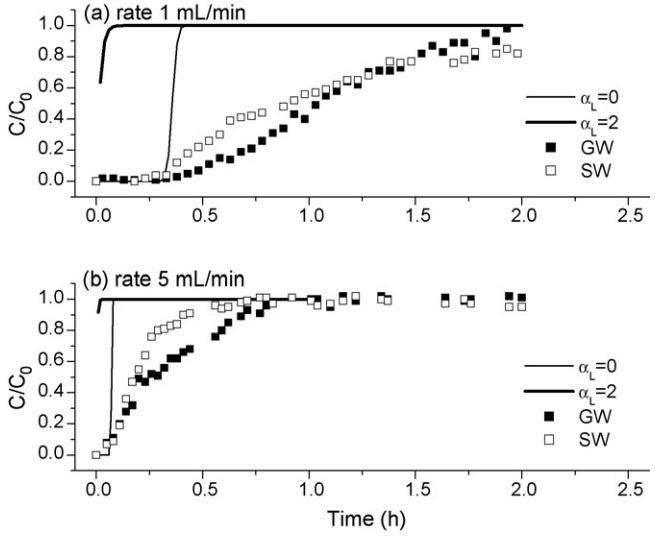

Fig. 4. The BTCs of HTO from 2 cm column and numerically fitted results. Solid lines indicate the model fitted BTCs.

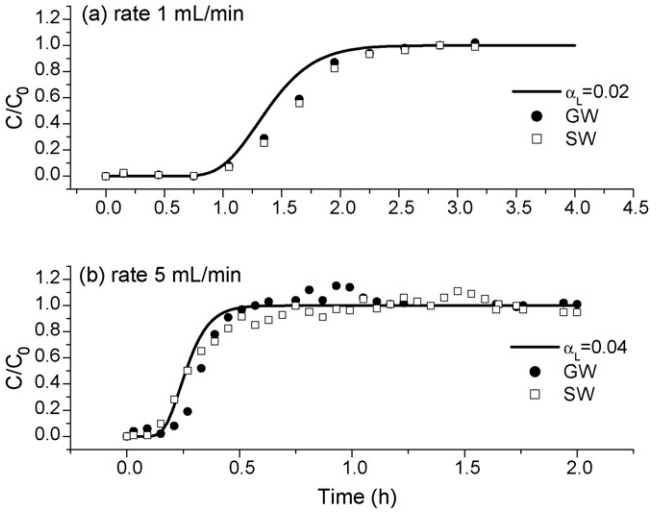

Fig. 5. The BTCs of HTO from 8 cm column and numerically fitted results. Solid lines indicate the model fitted BTCs.

To minimize discrepancies in numerical errors resulting from discretizations, the same grid size and time step size as in the 2 cm cases were applied for the 8 cm cases as mentioned previously. As shown in Fig. 5, the model requires the dispersivities of 0.02 dm and 0.04 dm at slow and fast flow rates, respectively, to fit the experimental 8 cm HTO BTCs. The determined dispersivities are slightly influenced by different flow rates as described in the literatures [22,23].

The significant tilting of 2 cm BTCs cannot be resolved even by given extremely large dispersivity. The question then arises of what factors can be attributed to the additional dispersive nature of BTCs in short columns. Fig. 1 shows that Teflon filter and ring are applied as supporting materials to both ends of the column. The sampling location for measuring the BTCs of column experiments is not immediately beside the bottom of the granite column. Thus it is necessary to consider whether these structures can be attributed to additional dispersive behaviors of the measured BTCs.

First the 0.8 cm thickness of the Teflon filter comprises evenly spaced 36 pin holes, each with a diameter of 2.5. These Teflon filters on both ends of the short column were simulated as the second type of porous medium with a porosity of 0.09, as estimated using 36 holes of 2.5 mm diameter on a 5 cm diameter cross section. Numerical experiments were conducted with a 3.6 cm column with two types of porous mediums, including a porosity of 0.09 with length of 0.8 cm on both ends and a crushed granite medium with porosity of 0.55 with length of 2 cm. No sorption is allowed in pores of Teflon filters. Results of numerical experiments still failed to reproduce the notably dispersive BTCs of 2 cm columns (figures not shown).

Second the 0.8 cm Teflon rings are further treated as the third type of porous medium, with porosity of 0.81, calculated as the inner diameter of the ring being 4.5 cm. No sorption is allowed in pores of Teflon filers and rings. Numerical experiments were then conducted using a 5.2 cm column with three types of porous mediums, including 0.8 cm Teflon rings and 0.8 cm Teflon filters on both ends of 2 cm packed crushed granite. Results were shown in Fig. 6 where the dispersivity of 1 mL/min flow rate is fitted as 0.001 dm and that of 5 mL/min flow rate is determined to be 0.02 dm. The dispersive 2 cm BTCs can be accurately captured when the additional dispersive effects caused by supporting materials were considered in modeling practices.

Although the 2 cm HTO BTCs can be manipulatively resolved by numerical models, questions arose regarding why the 8 cm BTCs can be simulated without considering the supporting materials. This

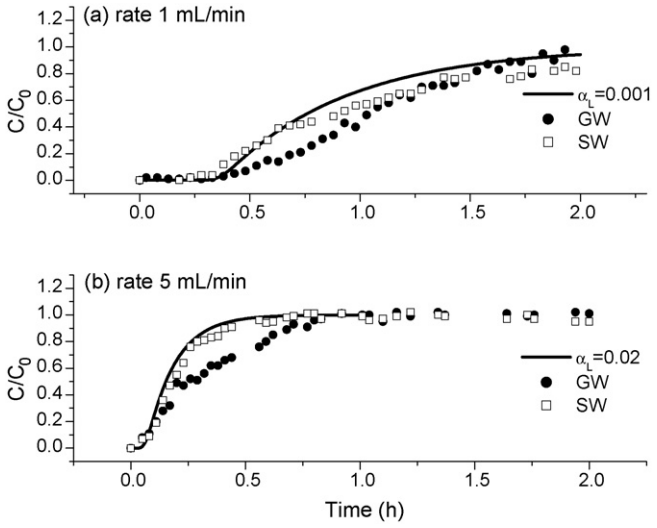

Fig. 6. The BTCs of HTO from 2 cm column fitted by considering the dispersive effects of Teflon filters and rings. Solid lines indicate the model fitted BTCs.

question can be answered in two ways. First the total length of supporting Teflon materials is 3.2 cm, which exceeds the pack crushed granite length of 2 cm, but is shorter than the long column of 8 cm. Structure induced dispersive behaviors significantly influence the tilting BTCs of short columns. Second the pore volume ratios of supporting Teflon materials to packed crushed granite are 1.31 and 0.33 for the 2 cm and 8 cm columns, respectively. Dispersive mixing of fluid before and after entering the short column might contribute to the tilting of BTCs. Consequently, the induced dispersive behaviors on BTCs by supporting materials are not negligible in short columns. Although this superfluous dispersive effect might be alleviated by increasing the flow rate to enhance advection, the numerical BTCs are still inadequate to represent the transport behavior of experimental BTCs in 2 cm cases. Besides fast flow rates might introduce additional uncertainties, such as particle cracking caused by high pore velocities. As presented in this study, even the flow rate was increased from 1 mL/min to 5 mL/min, the 2 cm HTO BTCs still cannot be resolved by numerical simulations. The dispersive effects associated with supporting structures can only be neglected when the column is sufficiently long as examined by numerical experiments.

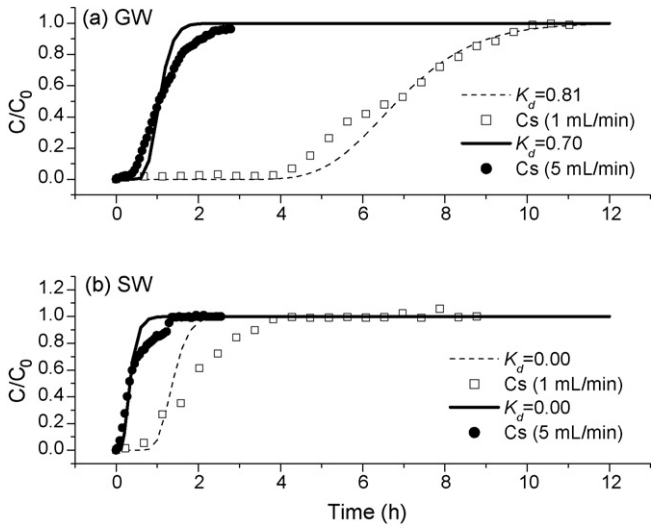

Fig. 7. The fitting of Cs BTCs for 8 cm column. Solid and dash lines indicate the model fitted BTCs.

Table 3
Comparisons of retardation factors determined from experiment data and model fitting of 8 cm column BTCs

Solution	Flow rate (mL/min)	K_d (mL/g)	R (experiment)	R (model)
CsGW	1	0.81	3.80	3.14
	5	0.70	3.18	2.85
CsSW	1	0.00	0.94	1.00
	5	0.00	1.22	1.00

3.3. Modeling BTCs of cesium

Since the BTCs of short column are contaminated by the dispersive behaviors of column supporting materials, numerical simulations of Cs BTCs are conducted using results of long columns. As shown in Fig. 7(a), the K_d values in GW are quantified as 0.81 g/mL and 0.70 g/mL for slow and fast flow rates, respectively. The numerically determined K_d values are slightly affected by flow rate variance. This phenomenon might be attributed to the limited time available for Cs nuclide to diffuse into the pores of crushed granite and thus the affinity of granite toward Cs nuclide is slightly reduced. On the other hand, the fitting of Cs BTCs in SW shows no retardation with the setting of zero K_d value as depicted in Fig. 7(b). It is the fact of impeded sorption by high potassium concentration which is in good agreement with that Cs adsorption is strongly sensitive to ionic strength in solutions [24–27].

Table 3 compares retardation factors determined based on the time ratio of Cs to HTO reaching half relative concentrations in experimental BTCs (as given in Table 2) and calculated from numerically retrieved K_d values with Eq. (3). In the case of the GW solution, both experimental R values slightly exceed those from the modeling. Furthermore, in the SW cases, the R values from modeling are given as unity as the associated K_d value of zero.

3.4. Modeling short column BTCs with long column parameters

Short column BTCs were further simulated with parameters determined from long columns. The dispersivities are set as 0.02 dm and 0.04 dm for slow and fast flow rates, respectively, as determined from 8 cm HTO BTCs. Only the 2 cm packed crushed granite is considered for simulations. As shown in Fig. 8, model reproduced Cs BTCs achieve breakthrough earlier than observed BTC suggesting

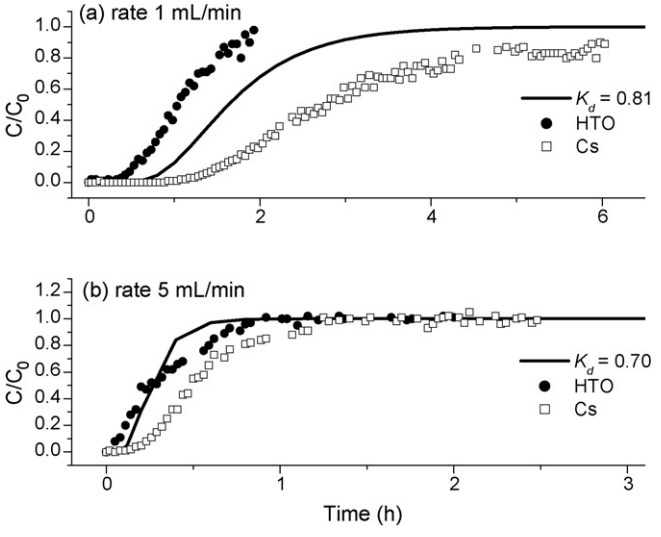

Fig. 8. Simulating the Cs and HTO transport in 2 cm with GW solutions by using the K_d values determined from 8 cm columns. Solid lines indicate the model fitted BTCs.

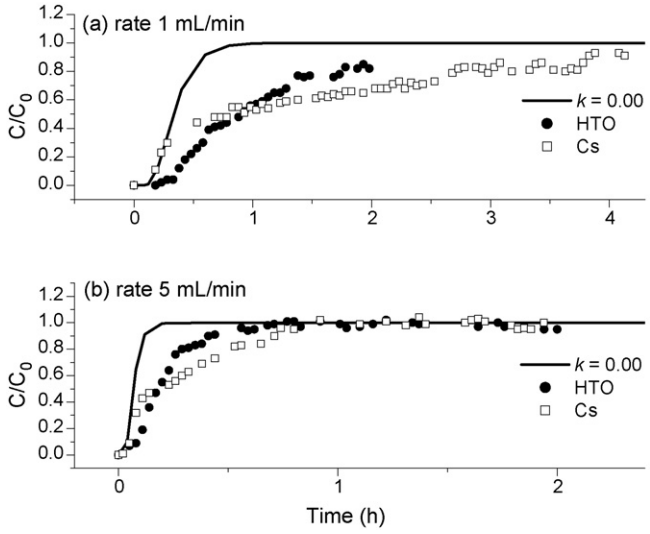

Fig. 9. Simulating the Cs and HTO transport in 2 cm with SW solutions by using the K_d values determined from 8 cm columns. Solid lines indicate the model fitted BTCs.

that over retardation would be wrongfully concluded from short column BTCs. Fig. 9 shows the results of model reproduced Cs BTCs in SW with a zero K_d as given in long column cases. The breakthrough of modeled BTCs is even early than those of observed BTCs. This phenomenon provides strong evidence supporting the suspicion that the 2 cm BTCs are contaminated by dispersion from column supporting structures. Incorrect information can be retrieved from the short column without cross examination with results from the long column and from numerical experiments. The structural dispersion is commonly ignored but seriously affects the determination of physical and chemical parameters when the column is short. Even with fast flow rate, the BTCs of short column may still be contaminated by dispersive transport of column supporting materials.

4. Conclusions

Experimental and numerical investigations of the effect of column lengths on retardation factor determination were conducted for cesium transport in crushed granite. This study examined the validity of BTCs from packed granite columns with different lengths and flow rates for both HTO and Cs in GW and SW. A series of numerical experiments clearly demonstrated that the BTCs from short columns are highly vulnerable to dispersive behaviors induced by mixing and transport through column supporting materials. Results of short column BTCs overestimated dispersivity and underestimated retardation factors. With strong advection of using fast flow rate, the influence of dispersive transport of column supporting materials on short column BTCs still cannot be ignored. To reduce the influence of structural dispersivity on the determination of retardation factors, the equivalent pore volume of column supporting materials should be smaller than those of packed porous medium. In addition, the total length of column supporting structures should be shorter than that of porous medium. Accordingly, using the long column and checking with numerical simulations is suggested before conducting further experiments to obtain valid and representative parameters for field applications.

Acknowledgements

The authors would like to thank the Nuclear Backend Management Department of the Taiwan Power Company and the Energy and Resources Laboratories at the Industrial Technology Research Institute for financially supporting this research. Ted Knoy is appreciated for his editorial assistance.

References

[1] K.V. Ticknor, T.T. Vandergraaf, The Treatment of Sorption and Retardation in the Assessment of Geological Barriers to Contaminant Transport, AECL-11698 Report, Geochemistry Research Branch, Whiteshell Laboratories, Manitoba, Canada, 1997.
[2] C. Zhu, D.S. Burden, Mineralogical compositions of aquifer matrix as necessary initial conditions in reactive contaminant transport models, J. Contam. Hydrol. 51 (2001) 145–161.
[3] S. Staunton, C. Dumat, A. Zsolnay, Possible role of organic matter in radiocaesium adsorption in soils, J. Environ. Radioact. 58 (2002) 163–173.
[4] P.D. Glynn, Modeling Np and Pu transport with a surface complexation model and spatially variant sorption capacities: implications for reactive transport modeling and performance assessments of nuclear waste disposal sites, Comput. Geosci. 29 (2003) 331–349.
[5] I. Gurban, M. Laaksohariju, B. Made, E. Ledoux, Uranium transport around the reactor zone at Bangombe and Okelobondo (Oklo): examples of hydrogeological and geochemical model integration and data evaluation, J. Contam. Hydrol. 61 (2003) 247–264.
[6] J.E. Saiers, G.M. Hornberger, Migration of 137Cs through quartz sand: experimental results and modeling approaches, J. Contam. Hydrol. 22 (1996) 255–270.
[7] M. Ochs, M. Boonekamp, H. Wanner, H. Sato, M. Yui, A quantitative model for ion diffusion in compacted bentonite, Radiochim. Acta 82 (1998) 437–443.
[8] I. Porro, M.E. Newman, F.M. Dunnivant, Comparison of batch and column methods for determining strontium distribution coefficients for unsaturated transport in basalt, Environ. Sci. Technol. 34 (2000) 1679–1686.
[9] J.A. Davis, J.A. Coston, D.B. Kent, C.C. Fuller, Application of the surface complexation concept to complex mineral assemblages, Environ. Sci. Technol. 32 (1998) 2820–2828.
[10] H.P. Cheng, M.H. Li, S. Li, A sensibility analysis of model selection in modeling the reactive transport of cesium in crushed granite, J. Contam. Hydrol. 61 (2003) 371–385.
[11] E. Worch, Modelling the solute transport under nonequilibrium conditions on the basis of mass transfer equations, J. Contam. Hydrol. 68 (2004) 97–120.
[12] A.J. Rabideau, J. Van Benschoten, A. Patel, K. Bandilla, Performance assessment of a zeolite treatment wall for removing Sr-90 from groundwater, J. Contam. Hydrol. 79 (2005) 1–24.
[13] H.M. Bekhit, A.E. Hassan, R. Harris-Burr, C. Papelis, Experimental and numerical investigations of effects of silica colloids on transport of strontium in saturated sand columns, Environ. Sci. Technol. 40 (2006) 5402–5408.
[14] N. Solovitch-Vella, J.M. Garnier, P. Ciffroy, Influence of the colloid type on the transfer of Co-60 and Sr-85 in silica sand column under varying physicochemical conditions, Chemosphere 65 (2006) 324–331.
[15] M.S. Rodriguez-Cruz, M.J. Sanchez-Martin, M.S. Andrades, M. Sanchez-Camazano, Modification of clay barries with a cationic surfactant to improve the retention of pesticides, J. Hazard. Mater. 139 (2007) 363–372.
[16] D. Langmuir, Aqueous Environmental Geochemistry, Prentice Hall, 1997.
[17] G.T. Yeh, M.D. Siegel, M.H. Li, Numerical modeling of coupled variably saturated fluid flow and reactive transport with fast and slow chemical reactions, J. Contam. Hydrol. 47 (2001) 379–390.
[18] D.R. Lide (editor-in-chief), CRC Handbook of Chemistry and Physics, 73rd ed., CRC Press, Florida, 1992.
[19] M. Jansson, T.E. Eriksen, In situ anion diffusion experiments using radiotracers, J. Contam. Hydrol. 68 (2004) 183–192.
[20] P.A. Domenico, F.W. Schwartz, Physical and Chemical Hydrology, Wiley, New York, 1997.
[21] S. Mascioli, M. Benavente, D.E. Martinez, Estimation of transport hydraulic parameters in loessic sediment, Argentina: application of column tests, Hydrogeol. J. 13 (2004) 849–857.
[22] M. Hauns, P.Y. Jeannin, Q. Atteia, Dispersion, retardation and scale effect in tracer breakthrough curves in karst conduits, J. Contam. Hydrol. 241 (2001) 177–193.
[23] S.E. Silliman, Laboratory study of chemical transport to wells within heterogeneous porous media, Water Resour. Res. 37 (2001) 1883–1892.
[24] C. Papelis, Cation and anion sorption on granite from the Project Shoal Test Area, near Fallon, Nevada, USA, Adv. Environ. Res. 5 (2001) 151–166.
[25] J.M. Zachara, S.C. Smith, C.X. Liu, J.P. Mckinley, R.J. Serne, P.L. Gassman, Sorption of Cs+ to micaceous subsurface sediments from the Handford site, USA, Geochim. ET Cosmochim. Acta 66 (2002) 193–211.
[26] C. Liu, J.M. Zachara, S.C. Smith, A cation exchange model to describe Cs^+ sorption at high ionic strength in subsurface sediments at Hanford site, USA, J. Contam. Hydrol. 68 (2004) 217–238.
[27] J.P. McKinley, J.M. Zachara, S.M. Heald, A. Dohnalkova, M.G. Newville, S.R. Sutton, Microscale distribution of cesium sorbed to biotite and muscovite, Environ. Sci. Technol. 38 (2004) 1017–1023.